Phys Chem Minerals (2006) 33: 332–346
DOI 10.1007/s00269-006-0084-z

ORIGINAL PAPER

Chung-Cherng Lin · Lin-gun Liu

Composition dependence of elasticity in aluminosilicate glasses

Received: 11 April 2005 / Accepted: 27 February 2006 / Published online: 4 April 2006

Abstract The elastic properties of two types of aluminosilicate (basaltic and rhyolitic) glasses have been studied using both Brillouin and Raman spectroscopy at ambient conditions. It has been found that the elastic moduli of the basaltic glasses decrease with increasing SiO_2 concentration. The shear moduli displayed the least dependence on SiO_2 content. The bulk moduli of the basaltic glasses strongly depend on the sum of the Q^3 and Q^4 anionic units. Among the modifiers, iron cations showed the strongest effect on the elastic properties of the rhyolitic glasses. For the elastic moduli of rhyolitic glasses, the major effect of alkaline earth cations is on shear modulus; however, both iron and alkali cations showed stronger effects on bulk modulus and similar relative contribution between bulk and shear moduli (based on the equivalent M^+ cation). The dependences of elastic moduli on bulk NBO/T observed in both types of glasses suggest that the elastic modulus of an aluminosilicate glass depends on the concentration of effective modifying cations rather than the apparent concentration of all non-network-forming cations. An analysis of data also indicated that the ideal molar mixing model is failed in prediction of the elastic properties of the present multicomponent glasses by using the known parameters.

Keywords Aluminosilicate glasses · Elastic properties · Glass structure · Brillouin scattering · Raman spectroscopy

Introduction

The presence of aluminum in a silicate glass has generally yielded a higher strain point, annealing and glass transition temperatures, and viscosity. Therefore, aluminosilicate glasses are important, both commercially and naturally (volcanic glasses). The effects of different components on the properties of a glass have been widely reported (e.g. Bansal and Doremus 1986). However, most of the studies have focused on simple systems (binary and ternary) rather than complicate multi-component glasses, e.g., volcanic. Study of the properties of volcanic glasses or melts is attractive due to its significance to our understanding of volcanic activities, diagenesis of igneous rocks, and the cause of seismic low-velocity zones in the mantle.

Besides nuclear magnetic resonance (NMR), the structure of silicate and aluminosilicate melts and glasses at various temperatures and pressures has been extensively studied using Raman spectroscopy (e.g. Mysen et al. 1980a; Stebbins et al. 1985; McMillan and Wolf 1995). Recently, temperature effects on elasticity of iron-free aluminosilicate glasses or melts have also been studied using Brillouin scattering by Askarpour and Manghnani (1993), Vo-Thanh et al. (1996) and Schilling et al. (2001, 2003). Thus, the dependence of elasticity on the silicate anionic structure, which is also composition-dependent, in a glass should be investigated. In addition, the relative contribution of non-network-forming cations to the elastic moduli of a multi-component aluminosilicate glass has not been reported, though the dependences of elastic properties on the concentration of network modifiers in simpler glasses have been widely studied (e.g. Schroeder et al. 1973; Rouse et al. 1981; Vaills et al. 1996; Burkhard 1997). It also remains unclear if the elastic moduli of a glass depend on only the apparent concentration of all non-network-forming cations.

To address these issues, we combined both Brillouin scattering and Raman spectroscopic studies to explore the effects of composition and structure on the elasticity of multi-component aluminosilicate glasses. Two types of simulated volcanic glasses, basaltic and rhyolitic (i.e., granitic), were used in this study. The former was used to study the effect of anionic structure (via changing SiO_2 concentration) on the elasticity of glass; the latter

C.-C. Lin (✉) · L. Liu
Institute of Earth Sciences, Academia Sinica,
Taipei 115, Taiwan, Republic of China
E-mail: cclin@earth.sinica.edu.tw
Fax: +886-2-27839871

was used to reveal the effects of concentration and types of cations on the elasticity of a complicate glass.

Experimental

Preparation of glasses

The composition of all samples is listed in Table 1. Samples*B*0–*B*3 are basaltic glasses and *B*1 has a typical composition of basalt, and it represents the average composition of 1,010 natural tholeiite and olivine tholeiite reported by Mysen (1987). Except for SiO_2, the relative amounts among other constituents in the basaltic glasses are the same. Samples G0–G3 are rhyolitic glasses, and *G*0 represents the average of 367 natural rhyolites (Mysen 1987). The Al_2O_3/SiO_2 molar ratio is same for all rhyolitic glasses, but is different for all basaltic glasses. The effects of SiO_2 on the anionic structure and elastic properties of glasses was studied using the basaltic glasses, while the effects of iron, alkaline earth, and alkali cations were estimated using the rhyolitic glasses.

Instead of P_2O_5, MnO, Na_2O and K_2O, high-purity $Na_3PO_4 \cdot 12H_2O$, $MnCO_3$, Na_2CO_3, and K_2CO_3 were used to prepare the samples. The total sodium was from both $Na_3PO_4 \cdot 12H_2O$ and Na_2CO_3. To obtain a better mixing, all oxides, carbonates, and phosphate were ground in an alumina mortar for 30 min at least. In order to remove CO_2 and H_2O, the mixtures were put into platinum containers and calcined at 1,300°C for 2 h for the basaltic samples and 3 h for the rhyolitic samples. The sample charges were then quenched to room temperature and pulverized for further mixing. Finally, different sample charges were fired in a CO/CO_2 atmosphere at different temperatures for different time durations (1,300°C, 3 h for *B*0 and *B*1; 1,350°C, 3 h for *B*2; 1,450°C, 5 h for B3; 1,550°C, 6 h for *G*0, *G*1, and *G*2, and 1,600°C 4 h for *G*3), and then quenched in air from 1,200°C for basaltic samples and from ca. 1,550°C for rhyolitic samples to room temperature on a brass plate. In order to control the oxidation state of iron, the partial pressure of oxygen (P_{O_2}) used during preparation of the samples was maintained in the range between the equilibria of FeO/Fe_2O_3 and Fe/FeO. However, the CO/CO_2 ratio was controlled by adjusting the relative flow rates of gases using mass flow controllers. Thus, the fugacity of O_2 during preparation of the samples would be not as precise as that controlled by a ZrO_2 oxygen sensor. It has been known that the change of composition in a glass caused by firing is generally rather small (e.g. Lange and Carmichael 1987) at a suitable firing temperature, and the change of mass is mainly caused by the loss of alkali elements due to weak M–O bond strength (M = cation). For the present samples, the mass losses in all sample charges are less than 0.4 wt% after firing. The mass change is attributed to the evaporation of some alkali (especially Na) and probably iron oxides, and it should, in term, cause less than 0.01 decrease in bulk NBO/T of the glasses. Thus, we did not analyze the final composition of the samples and used the composition listed in Table 1 in all calculations. Furthermore, the strongest characteristic Raman bands of carbonate group are at 1,070–1,100 cm^{-1} (v_1) and 700–720 cm^{-1} (v_4). We did not find any recognizable signal at these regions in Raman spectra of all samples. Therefore, we assumed all CO_3^{2-} ions have been decomposed during preparation of samples.

Characterization and NBO/T of samples

It has been known that both Ti and P can promote the polymerization of a silicate melt or glass (e.g. Kushiro 1975; Mysen et al. 1980b, 1981a; Ryerson 1985). Thus, like Si, both Ti and P are treated as network formers in a silicate glass. Al^{3+} has been found to have different coordination numbers in SiO_2–Al_2O_3 and alkali-free aluminosilicate glasses and melts (e.g. Yamane and Okuyama 1982; Poe et al. 1992). It is also known that all

Table 1 Composition (mol%), bulk NBO/T and density (g/cm^3) of the aluminosilicate glasses

	Basaltic				Rhyolitic			
	*B*0	*B*1	*B*2	*B*3	*G*0	*G*1	*G*2	*G*3
SiO_2	42.000	52.330	61.000	70.000	79.334	80.744	81.160	85.716
Al_2O_3	11.653	9.577	7.835	6.027	8.886	9.044	9.091	9.601
Fe_2O_3	1.705	1.401	1.146	0.882	0.786	–	0.804	0.849
FeO	8.509	6.994	5.722	4.401	0.961	–	0.983	1.038
MnO	0.189	0.155	0.127	0.098	0.056	0.057	0.057	0.061
MgO	15.305	12.580	10.292	7.917	0.675	0.687	–	0.730
CaO	14.270	11.728	9.595	7.381	1.574	1.602	–	1.701
Na_2O	3.504	2.880	2.356	1.812	4.338	4.415	4.437	–
K_2O	0.702	0.577	0.472	0.363	3.108	3.163	3.179	–
TiO_2	1.970	1.619	1.325	1.019	0.249	0.254	0.255	0.269
P_2O_5	0.194	0.159	0.130	0.100	0.033	0.033	0.034	0.035
Bulk NBO/T	1.045	0.792	0.608	0.439	0.084	0.016	0.067	0.111
Density[a]	2.923	2.881	2.682	2.552	2.471	2.282	2.423	2.355

[a]The densities were measured at 23 ± 1°C

Al^{3+} are tetrahedrally coordinated if enough charge-balance cations (e.g., alkali and alkaline-earth cations) are available in a silicate melt or glass (e.g. Taylor and Brown 1979; Mysen et al. 1981b; Navrotsky et al. 1982; McMillan et al. 1982; Domine and Piriou 1986; Mysen 2003). Therefore, except for G3, Al^{3+} was treated as a network former in all samples because of the presence of enough Na^+, K^+, Mg^{2+} and Ca^{2+} in these samples (see Table 1). In the case of G3, about 37.8% of Al^{3+} were considered to be network modifier because of the lack of charge-balance cations (Mysen et al. 1981b). Thus, G3 has the least effective Al^{3+} network former among the rhyolitic glasses. Fe^{3+} can be a network former and/or modifier. The $Fe^{3+}/\sum Fe$ molar ratio of all basaltic samples is 0.286, but is 0.621 for the three iron-bearing rhyolitic samples (G0, G2, G3). On the basis of Mössbauer spectroscopic studies (Mysen 1987), all Fe^{3+} can be assumed to be modifiers in the basaltic glasses and be network formers in the rhyolitic glasses. On the other hand, it has also been pointed out that Fe^{3+} is octahedrally coordinated in acidic Na_2O–SiO_2 glasses (and melts) if the Na/Si molar ratio is smaller than unity (Schreiber et al. 1994). Thus, Fe^{3+} in our rhyolitic samples was treated as modifier because Na/Si ratios in these glasses are all smaller than 0.2. The other cations (Na^+, K^+, Mg^{2+}, Ca^{2+}, Mn^{2+}, and Fe^{2+}) act as modifiers and/or the charge-balance cations of Al^{3+}, Fe^{3+}, and P^{5+}. Mysen (1987) suggested that the preferred cation for balancing the charge of P^{5+} is Ca^{2+}, and that the tendency for a cation to balance the charge of Al^{3+} has the order: $K^+ > Na^+ > Ca^{2+} > Fe^{2+} > Mg^{2+}$. The number of bulk non-bridging oxygens per each tetrahedrally coordinated cation (i.e., bulk NBO/T, T = Si, Al, P, Ti) listed in Table 1 were then calculated according to the above assumptions.

The glass transition temperatures (T_g) of the quenched basaltic glasses were determined to be 670–680°C using a differential scanning calorimeter (DSC) at a heating rate of 10°C/min in N_2(g) (Netzsch DSC 404). T_g's of the rhyolitic glasses should be generally higher than those of the basaltic glasses due to far more SiO_2. However, we failed to determine T_g for all rhyolitic glasses up to 1,000°C. This might be due to weak thermal effect in the rhyolitic glasses. It has been found that the internal stress (or strain) caused by quenching can deteriorate the elastic modulus of a glass (e.g. Gavriliu 2001; Vaills et al. 2001). To minimize the interference from internal stress, all quenched glasses in this study were annealed at 610°C for one hour. The reason for annealing samples at a temperature lower than T_g is to avoid devitrification during prolonged heat treatment. In addition, it has been found that the relaxation times of some glasses at their T_g's are only several minutes (e.g. Vaills et al. 2001; Le Saoût et al. 2002). Hence, the annealing at 610°C for 1 h was considered to be suitable for releasing stress in our basaltic glasses and probably in the rhyolitic glasses as well. All annealed iron-bearing glasses, except for *G*1 which is colorless and transparent, are dark-brown in color. All polished slices of annealed samples appeared to be homogeneous under polarizing microscope, except for *B*0 and *G*3. Minute square and black crystals up to 10–20 μm have been found in *B*0. A Raman analysis confirmed that these crystals are Fe_3O_4, indicating that the P_{O_2} during preparation of the samples might be close to the value for the equilibrium between Fe_3O_4 and ($FeO + Fe_2O_3$). However, the exact contents of Fe^{2+} and Fe^{3+} in the annealed samples were not determined. A layer of acicular crystals ca. 200 μm in thickness was found on the surface of *G*3 that was exposed to atmosphere during preparation of glasses. The acicular crystals in *G*3 should be formed during quenching, while Fe_3O_4 in *B*0 would be formed during firing. The remaining glassy region in *G*3 is homogeneous. Local devitrification in *B*0 and *G*3 may not have appreciable effect on the glass structure but might affect elastic properties of the glasses. Based on the volumes of the as-prepared glasses and the distribution and thickness of the crystals, the amounts of crystals in *B*0 and *G*3 are roughly estimated to be around 2 vol%. The presence of Fe_3O_4 crystals and the acicular crystals did not considerably interfere with the spectroscopic measurements because all Raman and Brillouin spectra were collected from the glassy region at the positions far from crystals. The densities of all annealed samples were measured by the Archimedean method at room temperature (23 ± 1°C).

Measurement of anionic structure and elasticity

The structure of the annealed glasses was probed using Raman spectroscopy. The unpolarized Raman signals were excited by the 514.5-nm line from an argon-ion laser and collected by a micro-Raman spectroscope (Jobin Yvon, LabRam HR) under backscattering (180°) geometry. The spectra were recorded at room temperature with an Olympus SLM Plan ×20 microscope objective and three accumulations at 60 s integration time with ~16 mW power on the samples. The focused laser spot on samples was estimated to be 4 μm in diameter. Wave numbers are accurate to ±1 cm^{-1} as determined from plasma emission lines. The frequency and intensity of each Raman band were estimated by the Jandel Scientific Peakfit computer software based on the assumption of Gaussian peak profile. The method described by Mysen et al. (1982) was followed for peak fitting and estimation of the abundance of anionic structural units. The uncertainties for band frequency and the relative abundance (fractions) of anionic units (i.e., Q^n in Tables 2 and 3, $n = 1, 2, 3$) are ±5 cm^{-1} and ±5%, respectively. Two assumptions were adopted for calculating the relative abundance: (a) all Q species distributing randomly throughout the whole glass, and (b) the electronic polarizability of a Q species being independent of the glass composition.

The elasticity of samples was measured by Brillouin scattering at room temperature. For such experiments, the glass plates with size of ca. 2×3 mm^2 and a thickness

Table 2 Fitted frequencies (cm^{-1}) and assignments for Raman bands in the basaltic glasses at ambient conditions

Assignments	*B*0	*B*1	*B*2	*B*3
Stretching of cation against oxygen cage[a]				294
Coupled vibration of M–O and SiO_4 network[a,b]			351	363
Out-of-plane motion of bridging oxygen[a,c]	426	426	429	424
Asym. deformation of Q^4 (rocking of bridging oxygen)[c]		460	463	457
Si–O–Si bending of four-membered siloxane ring of SiO_4 [a]	484	498	494	498
Si–O–Si vibration involving oxygen motion perpendicular to the Si···Si line[a]	544	549	550	554
Rocking motion of bridging oxygen in structural units that contain NBO[b]	575	574	574	573
Sym. Si–O–Si bending of three-membered siloxane ring of $(Al,Si)O_4$ tetrahedra[a]	585			
Oxygen bending with some contribution from Si atom[b,c]	713	740	774	803
Sym. stretching of Q^1 [c,d] and/or Ti–O stretching[e,f]	885 (0.23/0.32)	903 (0.35/0.42)	906 (0.31/0.30)	909 (0.32/0.32)
Sym. stretching of Q^2 [c,d]	948 (0.59/0.25)	964 (0.46/0.17)	961 (0.35/0.10)	962 (0.36/0.11)
Asym. stretching of bridging oxygen in all Q species[b]	1,012	1,023	1,015	1,027
Sym. stretching of Q^3 [c,d]	1,072 (0.17/0.43)	1,076 (0.19/0.42)	1,078 (0.34/0.59)	1,084 (0.32/0.57)
Asym. stretching of Q^4 with Si–O–Si = 160°[a–c]			1,169	1,163

Values inside the parentheses are the estimated relative abundance (fractions) among Q^1, Q^2, and Q^3. The left values were based on the intensity (peak area) of the fitted bands, and the right values were calculated by adopting both intensity and the normalized cross sections used by Mysen et al. (1982). The uncertainties for band frequency and the relative abundance of Q species are ± 5 cm^{-1} and $\pm 5\%$, respectively

Sym. symmetric, *Asym.* asymmetric, *NBO* non-bridging oxygen

[a]McMillan and Wolf (1995)
[b]Mysen et al. (1981b)
[c]Mysen et al. (1980a)
[d]Konijnendijk and Stevelts (1976)
[e]Furukawa and White (1979)
[f]Iwamoto et al. (1975)

of 25–35 μm were used. The polished opposite faces of the glass plates are parallel to each other within 0.5°. Specimens thus prepared were mounted on a goniometer head of an Eulerian cradle, and then were aligned to obtain a symmetric scattering geometry with an external angle of 90° between the incident and scattered beams. With this geometry, the refractive index can be cancelled out in the calculation of acoustic velocity (Whitfield et al. 1976). A 514.5-nm argon-ion laser and a six-passes tandem Fabry-Pérot interferometer (JRS Scientific Instruments) were used for the Brillouin experiments. A photomultiplier tube was used as the detector, and the

Table 3 Fitted frequencies (cm^{-1}) and assignments for Raman bands of the rhyolitic glasses at ambient conditions

Assignments	*G*0	*G*2	*G*3
(I) modifying cation–oxygen cage stretching[a] or (II) coupling of modifying cation-deformation of SiO_4 network[a,b]	333	323	333
Out-of-plane motion of bridging oxygen[a,c]	434	427	427
Asym. deformation of Q^4 (rocking of bridging oxygen)[c]	461	460	458
Si–O–Si bending of four-membered siloxane ring of SiO_4[a]	496	495	493
Si–O–Si vibration involving oxygen motion perpendicular to the Si···Si line[a]	542	544	527
Rocking motion of bridging oxygen in structural units that contain NBO[b]	589	593	595
(I) Si–O stretching with large Si displacement[a] (II) oxygen-bending motion with some contribution from Si[b,c]	799	796	803
Sym. stretching of Q^2 [c,d]	953	954	951
Asym. stretching of bridging oxygen in all Q species[b]	1,019	1,017	1,024
Asym. stretching of Q^4 with Si–O–Si = 120°[a,b,c]	1,042	1,046	1,064
Sym. stretching of Q^3 [c,d]	1,083	1,085	1,090
Asym. stretching of Q^4 with Si–O–Si = 160°[a,b,c]	1,150	1,142	1,161

The uncertainties for band frequencies are ± 5 cm^{-1}

[a]McMillan and Wolf (1995)
[b]Mysen et al. (1981b)
[c]Mysen et al. (1980a)
[d]Konijnendijk and Stevelts (1976)

free spectral range (FSR) and finesse were 29.9792 GHz and 120, respectively. To avoid crystallization caused by laser heating, the laser power on the specimen was lowered to 30 mW or less. For the 90° symmetric geometry, the acoustic velocity (V) can be calculated by the following formula (Whitfield et al. 1976):

$$V = \left(\frac{\Delta\omega\lambda}{2}\right)^{\frac{1}{2}}, \quad (1)$$

where $\Delta\omega$ is the Brillouin shift and λ the wavelength of the incident beam. As the treatment for Raman bands, each Brillouin frequency shift was estimated by assuming the Gaussian peak profile. In order to obtain better scattered signals, a Glan–Taylor prism was used to rotate the polarization of the incident laser beam to 45°. The bulk (K), shear (G), and Young's (E) moduli and Poisson's ratio (v) for the elastically isotropic materials were then calculated according to the following equations:

$$V_T = (C_{44}/\rho)^{1/2} = (G/\rho)^{\frac{1}{2}} \quad (2)$$

$$V_L = [C_{11}/\rho]^{\frac{1}{2}} = [(K + 4G/3)/\rho]^{\frac{1}{2}} \quad (3)$$

$$E = \frac{9K}{(1 + 3K/G)} \quad (4)$$

$$v = \frac{(1 - 2G/3K)}{(2 + 2G/3K)}, \quad (5)$$

where ρ is the density of sample, and V_T and V_L the transverse and longitudinal acoustic velocities, respectively. It should be noted that the elastic properties of a melt (or supercooled melt) consist of vibrational and configurational parts, the former is related to vibration of chemical bonds only and the latter involves relaxation of the melt. In such a case, the data collected by Brillouin scattering technique at an extremely high frequency (1–10 GHz) are only the vibrational contribution because relaxation cannot be probed at such a short time. However, the configurational part can be ignored at temperatures much below glass transition due to the translation and rotation of structural groups (i.e., relaxation) are not present. Therefore, the elastic properties of a glass determined by Brillouin and the low-frequency ultrasonic technique at room temperature are the same and both are vibrational.

For Brillouin scattering method, the transit time of the waves is too short to allow exchange of heat. Thus, the entropy is regarded to be constant during measurement, and the moduli obtained from Brillouin spectroscopy are all adiabatic. The adiabatic (K_S) and isothermal (K_T) bulk moduli are related by thermodynamic Grüneisen parameter (γ_{th}) and thermal expansion coefficient (α) as follows:

$$K_S/K_T = 1 + \gamma_{th}\alpha T. \quad (6)$$

The refractive indices for the basaltic glasses were determined using a 30/60° asymmetric scattering geometry with the external angle of 90° between the incident and scattered beams. The data collected from 45/45° symmetric scattering were adopted as references for calculation of refractive index. The refractive index (n) of an optically isotropic solid can be obtained according the following equation:

$$n = \left[\frac{A^2 - 3}{8A - 16}\right]^{\frac{1}{2}} \quad \text{and} \quad A = 4\left(\frac{\Delta v_i}{\Delta v_{45}}\right)^2 - \sqrt{3}, \quad (7)$$

where Δv_i and Δv_{45} are the Brillouin shifts obtained from 30/60° and 45/45° geometries, respectively. Both transverse and longitudinal signals were used in the calculation, and the final index for a given sample is the average of all data sets.

Results

Raman spectra of the aluminosilicate glasses

The structure of silicate glasses and melts has been widely studied using both ^{29}Si NMR and Raman spectroscopy. Although different structural units have been adopted to described the anionic structure of silicate glasses (e.g. Konijnendijk and Stevelts 1976; Karlsson and Fröberg 1987), a simpler set of anionic structural units has been widely used for this purpose; i.e., the so-called Q species used in NMR studies: SiO_4^{4-} (Q^0, monomer), $Si_2O_7^{6-}$ (Q^1, dimer), $Si_2O_6^{4-}$ (Q^2, chain), $Si_2O_5^{2-}$ (Q^3, sheet), and SiO_2 (Q^4, fully polymerized SiO_4 network). Note that Q^2 also represents a ring unit $Si_nO_{3n}^{2n-}$. Thus, we adopted this simple set of units throughout the study. Figure 1 shows Raman spectra of the basaltic glasses obtained in this study. Each spectrum can be divided into three regions: 300–650, 650–800, and 800–1,200 cm^{-1}. It is found that the Raman bands in all four spectra appeared to be significantly overlapped. This is attributed to the presence of Al^{3+} in the Q species.

The amounts of TiO_2 and P_2O_5 in the present samples are much less than that of SiO_2 and Al_2O_3. When the amounts of modifying cations are large enough, as in the present glasses, it has been pointed out that Ti and P can react with silicate complexes to coordinate metal cation via the following reactions to polymerize the silicate melt (e.g. Ryerson and Hess 1980; Mysen et al. 1980b):

$$\mathrm{Si-O-M-O-Si + Ti-O-Ti = Si-O-Si + Ti-O-M-O-Ti}$$

and

$$\mathrm{1.5\,Si-O-M-O-Si + PO_{2.5} = 1.5\,Si-O-Si + M_{1.5}PO_4},$$

where M denotes the modifying cation. These Ti- and P-bearing species have their own characteristic Raman signals (Furukawa and White 1979; Mysen et al. 1980b; Mysen et al. 1981a). After careful examination, we did not observe any Raman signal which can be attributed to the Ti- and P-bearing species, suggesting that the

effect of these species on the glass structure of our samples is negligible.

The extent of polymerization in a silicate glass can be described by the distribution of Q species. The characterized bands of Q^2 and Q^3 are included in the envelope of 800–1,200 cm^{-1}, while the representative bands for pure amorphous silica (equilvant to Q^4) are at ~430, 1,060, and 1,190 cm^{-1} (e.g. Galeener 1979). However, bands at both 1,060 and 1,190 cm^{-1} for amorphous silica are rather weak (Galeener 1979). Therefore, we neglected the two bands in the fitting process for the less polymerized samples ($B0$ and $B1$). In addition to the Q^2- and Q^3-related bands, at least two other bands centered at ~900 and ~1,020 cm^{-1} were demanded to get a good deconvolution for the 800–1,200-cm^{-1} envelope. The fitted frequencies and assignments of the bands and the relative abundance (fractions) of Q species based on the band intensities of Q^1, Q^2, and Q^3 are listed in Table 2.

Only one band was assigned in the region 650–850 cm^{-1}. This band should be equivalent to the 800-cm^{-1} band in amorphous silica although it may be complicated by overlapping with the vibrations from Ti-related units (e.g., O–Ti–O deformation), if any. With increasing Al_2O_3 content, the frequency of this band was significantly lowered in concomitant with the increase in band intensity and width. The most important feature below 650 cm^{-1} is the band at ~430 cm^{-1}. This band is caused by out-of-plane motion of bridging oxygen and has at least three interpretations (McMillan and Wolf 1995): symmetric oxygen stretching of bent Si–O–Si, symmetric bending of Si–O–Si with oxygen motion perpendicular to the Sii···Si lines, and symmetric O–Si–O angular deformation of the coupled SiO_4 group. In addition, as listed in Table 2, the relative abundance of Q^3 decreases with decreasing SiO_2 content (or increasing bulk NBO/T), but it is inverse for Q^2. The abundance of Q^1 seems to be insensible in the composition range studied.

Raman spectra of the rhyolitic glasses are shown in Fig. 2. We failed to collect a good spectrum of the iron-free sample ($G1$) due to strong background. Only a weak bulge at 400–530 cm^{-1} in the spectrum of $G1$ was seen. The cause of this phenomenon is unclear, though it might involve the fluorescence from Mn^{2+}. The interaction between energy levels of Fe^{2+}/Fe^{3+} and Mn^{2+} might inhibit the fluorescence and enabled us to observe Raman signals of other rhyolitic samples. The basis and assumptions for deconvoluting Raman spectra of the basaltic glasses were also applied to the rhyolitic glasses. In Fig. 2, each spectrum is also divided into three regions: 200–650, 750–850, and 850–1250 cm^{-1}. Compared to the spectra of basaltic glasses, all Raman spectra of the rhyolitic glasses showed a better resolution and higher frequency in the high-frequency envelope (850–1,250 cm^{-1}). The blue shift indicates that the bands at 1,060 and 1,190 cm^{-1} for Q^4 cannot be ignored. We combined the two bands in the peak fitting, though the frequencies may not identical to those of pure silica. The fitted frequencies and assignments for the Raman bands of rhyolitic glasses are listed in Table 3. Because the purpose of our study of rhyolitic samples is to find out the effects of different ingredients, the relative abundance of Q species in these glasses was not estimated here.

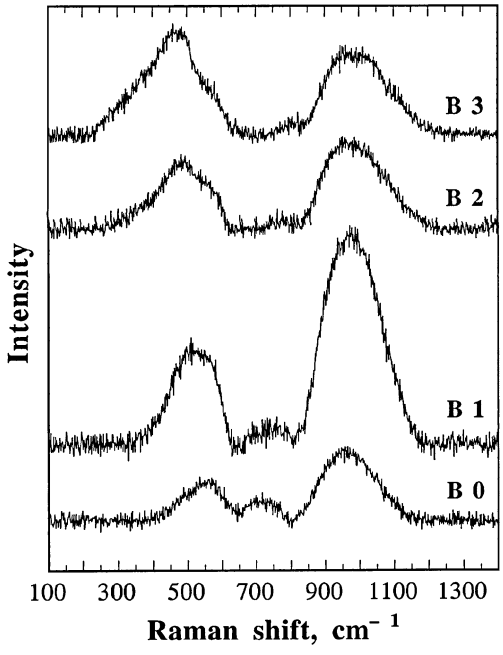

Fig. 1 Raman spectra of the basaltic glasses (unpolarized) at ambient conditions. The background for all spectra has been subtracted

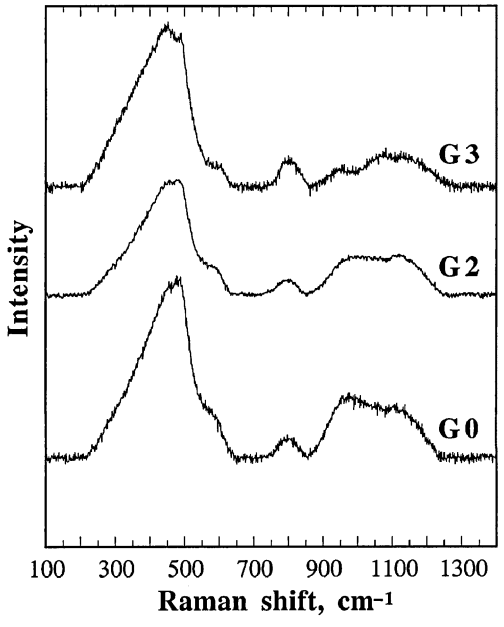

Fig. 2 Raman spectra of the rhyolitic glasses (unpolarized) at ambient conditions. The background for all spectra has been subtracted

Two possible interpretations were assigned for the broad band at 750–850 cm^{-1} (Table 3). This band should be equivalent to that at 710–805 cm^{-1} of the basaltic glasses, but far less influenced from Al^{3+}. In comparison with other rhyolitic glasses, both Q^3- and Q^4-related bands (at 1,064 and 1,161 cm^{-1}) in *G*3 showed higher Raman frequencies, accompanied with an increase in frequency and weakening in intensity for the band at 527–542 cm^{-1} (see Fig. 2 and Table 3). This confirms that the effective concentration of Al^{3+} network former in *G*3 is less than other rhyolitic glasses.

Elasticity

The SiO_2 dependence of elasticity for the basaltic glasses is displayed in Fig. 3a. Except for SiO_2, the relative concentrations of other oxide components were assumed to be the same for these samples, though the firing conditions for preparation of the samples were different. As shown, all three elastic moduli (bulk, shear and Young's) of the basaltic glasses decrease with increasing SiO_2 concentration. The Brillouin spectra of *B*0 were collected from the glassy region, though *B*0 contains some Fe_3O_4 crystals. Thus, the elastic moduli of *B*0 shown in Fig. 3a are not for glass/crystal composite. If the abscissa is changed to bulk NBO/T, as shown in Fig. 3b, it is found that the relationship between elastic moduli and bulk NBO/T is linear for *B*1–*B*3, and those for *B*0 are significantly below the linear trend. As would be expected, the deviation is attributed to low iron concentration in the glassy region of *B*0 (see Discussion). It is noteworthy that the abscissas adopted in Fig. 3a, b has different meanings; the former emphasizes the *apparent* effect of SiO_2 without other network-forming cations and the latter indicates the effect of *effective* modifying cations.

Figure 4 shows Poisson's ratios (v) for the basaltic glasses plotted as a function of SiO_2 concentration. Similar to binary alkali silicate glasses (Bansal and Doremus 1986), the Poisson's ratio of the basaltic glasses increases with decreasing SiO_2 concentration. The change in v from *B*0 to *B*3 is 15%, which is close to that in Young's modulus (14%). This behavior can be ascribed to that both correlate with the average stress and/or strain in a solid.

To ascertain the effect of different types of cation on the elastic properties of an aluminosilicate glass, we represented the elastic moduli of the rhyolitic glasses as a function of the bulk NBO/T rather than SiO_2 concentration in Fig. 5. Obviously, the elastic moduli of the rhyolitic glasses also increase monotonically with increasing bulk NBO/T. Note that the composition of samples *G*1–*G*3 is based on *G*0 with missing out one type of oxides for each sample. The molar ratio between any two ingredients is constant among all rhyolitic samples. By adopting *G*0 as a reference, the removal of iron oxides (*G*1) and alkaline earth oxides (*G*2) has caused a lowering in bulk, shear, and Young's moduli, but the reversal is found if alkali oxides (*G*3) are removed. In other words, the aluminosilicate glass can be strengthened by the addition of iron and alkaline earth cations and weakened by alkali cations.

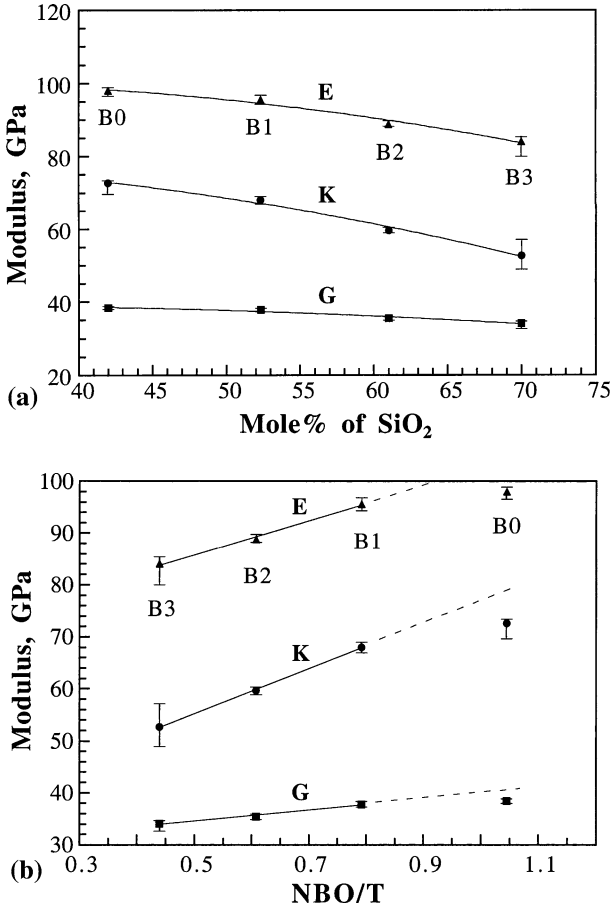

Fig. 3 Variations of bulk (*K*), shear (*G*) and Young's (*E*) moduli with **a** SiO_2 concentration and **b** bulk NBO/T in the basaltic glasses. Only the data of *B*1, *B*2 and *B*3 were used to fit the straight lines in (**b**). The *solid symbols* represent the average values

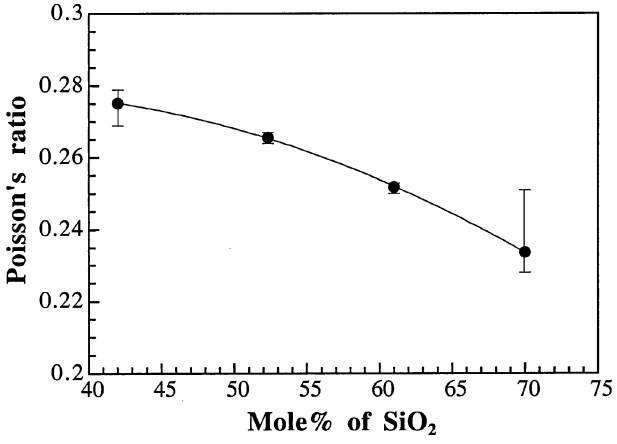

Fig. 4 Variations of Poisson's ratios with SiO_2 concentration in the basaltic glasses. The *solid circles* denote the average values

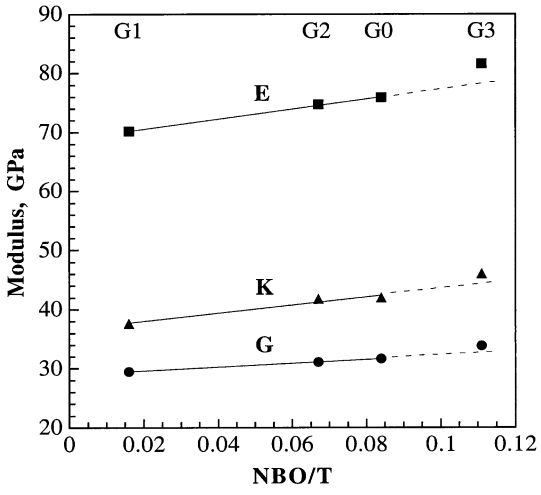

Fig. 5 Variations of bulk (*K*), shear (*G*) and Young's (*E*) moduli with bulk NBO/T in the rhyolitic glasses. The *solid symbols* represent the average values and the uncertainties for all data are within the symbols. Only the data of *G*0, *G*1 and *G*2 were used to fit the straight lines

Refractive index of the basaltic glasses

The refractive indices for the basaltic glasses are also plotted as a function of SiO_2 concentration in Fig. 6. The large uncertainty in refractive index is attributed to the method we adopted and the extent of transparency of samples. In comparison with the 45/45° geometry, Brillouin scattering experiment involving an asymmetric 90° geometry will result in smaller Brillouin shifts of the signals. Therefore, the quality of Brillouin signals would significantly affect the accuracy in fitting peak positions. The weak Brillouin signals of our samples are mostly due to the dark color. The weak signals have caused a larger uncertainty in fitting peak positions and that in turn resulted in a larger uncertainty in calculation of refractive index. A smaller uncertainty could be obtained by adopting backscattering because the Brillouin shift becomes n times (n = refractive index) that observed in the 45/45° geometry. The change of refractive index is only 2.5% from *B*0 to *B*3. Photon conduction is one of the mechanisms for heat transport in magma. The weak composition dependence of refractive index indicates that the change of radioactive heat does not cause a significant contribution to the heat transfer within a basaltic magma even if the composition is changed significantly.

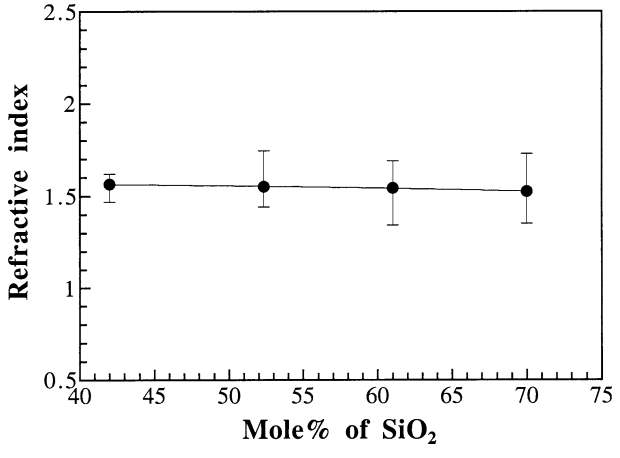

Fig. 6 Variations of refractive indices with SiO_2 concentration in the basaltic glasses. The *solid circles* denote the average values

Discussion

Structure of the aluminosilicate glasses

The basaltic glasses used in this work have the bulk NBO/T between 0.44 and 1.05. Therefore, the major equilibrium between Q species at T_g should be (without balance)

$$T_2O_5^{2-}(Q^3) = TO_2(Q^4) + T_2O_6^{4-}(Q^2),$$

where T is the tetrahedrally coordinated Si^{4+}, Al^{3+}, Ti^{4+}, and P^{5+} (the network-former cations). In order to get a good deconvolution for the 800–1,200-cm^{-1} envelope observed, as mentioned earlier, it requires to assign two additional bands centered at ~900 and ~1,020 cm^{-1}. In Table 2, based on the consideration of intensity, the band at ~900 cm^{-1} was very likely caused by the symmetric stretching of Q^1 unit, though the signal from Ti-related species cannot be totally excluded. Thus, an extra equilibrium between Q^2 and $(Q^1 + Q^3)$ should coexist at T_g.

As shown in Fig. 1, the 800–1,200-cm^{-1} envelope shifts to higher frequency with increasing SiO_2. This trend resulted from increasing relative abundance of Q^3 species and decreasing in NBO/T (see Table 2). The frequency of Q^3 also decreases with increasing bulk concentration of aluminum (see Table 1). This is due to the preferential substitution of Al^{3+} in Q^3 and Q^4 species (Mysen et al. 1981b; Mysen 2003).

The rhyolitic glasses are more polymerized than the basaltic glasses. As shown in Fig. 2, we did not observe any signal corresponding to Q^0 and Q^1 in all spectra. Thus, the equilibrium in the rhyolitic glasses at T_g is only between Q^3 and $(Q^2 + Q^4)$. The difference in the relative abundance of Q species among the glasses is negligible due to the small difference in bulk NBO/T. It is noticed that the relative intensity of Q^2 signal (at ~950 cm^{-1}) decreases from *G*0 to *G*3 (Fig. 2). This result may be correlated to the case that more Q^2 were produced due to preferred association of small M^+ and M^{2+} cations with Q^2 species suggested by McMillan (1984) (Note that there are no CaO and MgO in *G*2, and Na_2O and K_2O in *G*3). Probably, different coordination numbers of cations should also be considered for the intensity change of Q^2 (Li 2004).

Effects of anionic structure on elasticity

For the basaltic glasses, both bulk and Young's moduli show similar SiO_2 dependences and shear modulus displays the weakest dependence (Fig. 3a). All elastic moduli can be represented by $M = \rho f$, where M denotes the elastic moduli (K, G, E, and v), ρ the density, and f a function of acoustic velocities. In order to evaluate the contribution beyond the change of density, the elastic moduli of $B3$ were adopted as references and the data of other samples were normalized against those of $B3$ and plotted as a function of SiO_2 concentration in Fig. 7. Similar normalizing for the variation of density (the dotted line) is also shown in Fig. 7. If the redistribution of anion structural units can be neglected and the change in elastic properties of a glass due to composition change is only related to density, then the change in elastic properties should follows the variation of density (according to $M = \rho f$). Figure 7 reveals, however, that the change rate in shear modulus is slower than that of density, whilst those of both bulk and Young's moduli are greater than that of density. Furthermore, the variation of bulk modulus is much greater than those of both shear and Young's moduli. Thus, elastic moduli should be affected significantly by the change in glass structure.

The rapid rise of bulk modulus upon decreasing SiO_2 concentration indicates the presence of a strong dependence on the extent of polymerization of a glass. As mentioned earlier, the relative abundance of Q^3decreases with decreasing SiO_2 content, but it is inverse for Q^2. This should be, in term, accompanied a decrease in abundance of Q^4 as observed in other simpler systems (e.g. Mysen 1987; Li 2004), though the relative amount of Q^4 has not been estimated. Relative to the SiO_4 dimer (Q^1) and chain (Q^2), the geometric structure of Q^3 and Q^4 is looser due to irregular linking of TO_4 tetrahedra (T = Si, Al) and the presence of empty and cation polyhedra within the more polymerized structural units. In other words, both Q^1 and Q^2 themselves should contribute far smaller volume contraction to a glass under hydrostatic compression, and hence the bulk moduli of the present basaltic glasses strongly depend on the amount of (Q^3 + Q^4). A glass that contains more Q^3 and Q^4 should be more compressible. In addition to changes in bond angles and lengths of the cation polyhedra, shear deformation of a glass involves gliding between Q species. Both Q^3 and Q^4 species, rather than Q^1 and Q^2, would cause more steric hindrance during gliding. The presence of steric hindrance resists shear deformation of a glass and causes a smaller change in shear modulus. Therefore, the significant difference in change rates between bulk and shear moduli of the basaltic samples is originated from different mechanisms operating on compression and shear deformation. As shown in Fig. 7, the increase rate in Young's modulus with decreasing SiO_2 content is much close to that of density. This is comprehensible because density is a bulk property and Young's modulus is the constant correlates to the average strain and stress in a solid.

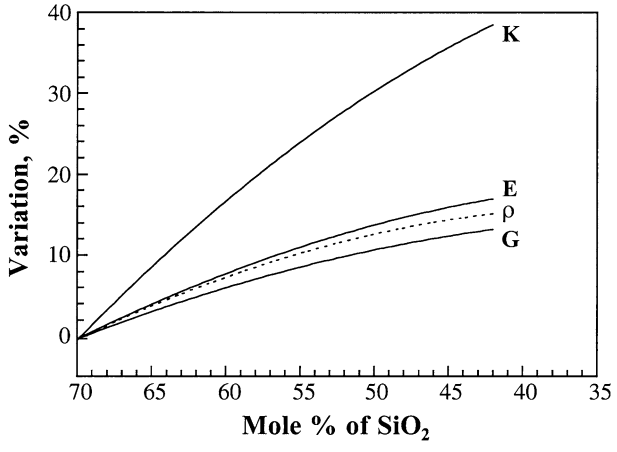

Fig. 7 The data of Fig. 3a are normalized against those of the glass having the lowest bulk NBO/T (i.e., $B3$). The variation of density (ρ) are also shown for reference

It should be noted that the results shown in Fig. 7 is valid only for the composition range studied. An extrapolation to pure silica for all moduli in Fig. 3a would yield elastic moduli that are much lower than those of amorphous silica. This suggests either that minimum moduli may exist, similar to that found in sodium silicate glasses (Lin et al. 2006), or that the change of moduli may become more rapid at higher silica region.

Composition dependence of elasticity

In Fig. 3b, as mentioned earlier, all the elastic moduli of the basaltic glasses display linear dependences on bulk NBO/T except for $B0$, and the addition of iron oxides has strengthened the multi-component aluminosilicate glasses. Similar strengthening effect was also observed in Fe^{3+}-bearing alkali silicate glasses (Burkhard 1997). The negative deviation from linear dependence for $B0$ (Fig. 3b) can be ascribed to the drop of effective concentration of iron ions in the glasses due to precipitation of Fe_3O_4. The bulk NBO/T in the glassy region of $B0$ was estimated to be ~0.9, should the elastic moduli of these basaltic glasses all follow a linear trend, i.e., ~36 % of the iron oxides were exsolved to form Fe_3O_4 crystals in $B0$.

For rhyolitic glasses (Fig. 5), the linear dependences between the elastic moduli and bulk NBO/T are apparent for $G0$–$G2$, and $G3$ shows a positive deviation from this linear trend. The acicular crystals grew only from the surface exposed to air upon quenching. The Brillouin data were collected from the area far from the surface layer. Thus, the high elastic moduli of G3 should be almost independent of the growth of acicular crystals. According to the assumptions adopted for calculating the bulk NBO/T, the modifiers in $G3$ should be the unbalanced Al^{3+} ions alone. The addition of Al_2O_3 in a

silicate glass should always cause an increase in elastic modulus (Bansal and Doremus 1986). Therefore, the higher moduli in *G*3 may result from the presence of more amounts of effective Al^{3+} modifiers.

In order to evaluate the quantitative contribution of different cations on the elastic moduli of aluminosilicate glasses, the data of *G*1, *G*2 and *G*3 were normalized against those of *G*0 in Table 4 based on equivalent concentrations of M^{+}. The percentage changes between *G*1 and *G*0 represent the total contribution of iron cations (Fe^{2+} and Fe^{3+}), those between *G*2 and *G*0 of alkaline earth cations (Mg^{2+} and Ca^{2+}), and those between *G*3 and *G*0 of alkali cations (Na^{+} and K^{+}). It is found that the differences in Young's modulus between *G*0 and other glasses are close to that in density. As pointed out earlier for the basaltic glasses, density is a bulk property and Young's modulus correlates average strain and stress in a solid. So, naturally, the variation of Young's modulus approximates that of density. Among the three types of cations, iron oxides show the strongest effect on the elastic moduli of aluminosilicate glasses (see the ΔM%/mol% of equivalent M^{+} in Table 4). This may be correlated to their strong field strength (Z/r^2, Z = charge, r = ionic radius). The major effect of alkaline earth cations is on shear modulus, and both iron and alkali cations showed stronger effects on bulk modulus. The apparently weak effect of alkali and alkaline earth cations on the elastic moduli may be correlated to all or a part of them is the charge-balance cations of Al^{3+} and P^{5+} and the loss of alkali elements during preparation of glasses. It is noteworthy that both iron and alkali cations show similar relative contributions between bulk and shear moduli (based on the equivalent M^{+} ion), though the two types of cations have the inverse effects on elastic moduli. This suggests that iron and alkali cations may have similar local structure or prefer to associate with the same anionic units in the glass. For alkaline earth cations, the large difference in contribution between bulk and shear moduli (Table 4) implies that Mg^{2+} and Ca^{2+} prefer to associate with Q^2 and Q^1 rather than the more polymerized Q^3 and Q^4; the latter two species are the key units for compression and, thus, bulk modulus.

For the basaltic glasses, the elastic moduli increase with increasing the apparently equivalent M^{+} concentration of all non-network-forming cations. However, such a regular dependence was not observed in the rhyolitic glasses if charge balance for Al^{3+} and P^{5+} are not considered. Thus, the monotonous variation of moduli with bulk NBO/T shown in Figs. 3b and 5 reveals that the elastic moduli of a glass strongly depend on the effective concentration of the modifying cations rather than on the apparent concentration of all non-network-forming cations.

A test to the ideal molar mixing model

To explore the bulk properties of magma and glasses, the ideal mixing of molar properties of oxides has been widely adopted. Accordingly, the property M can be calculated by $Q = \sum x_i Q_i$, where, x_i is the molar fraction of component i, and Q_i the corresponding molar properties. Three routes related to the prediction of the elastic properties of melts and glasses have been developed based on the ideal mixing model. The first involves the calculation of density from partial molar volumes (V_i) of component oxides which are determined by thermal expansion data of melts (e.g. Bottinga et al. 1982; Stebbins et al. 1984; Stein et al. 1986; Lange et al. 1987; Knoche et al. 1995; Lange 1996, 1997). The second directly estimates Young's modulus of glasses at ambient conditions based on theoretical consideration of packing density of atoms and dissociation energy of *crystalline* oxides (Makishima and Mackenzie 1973; Rocherulle et al. 1989; Inaba et al. 1999). The third uses a set of sound speed coefficients (C_i) for oxides at high temperatures (Rivers and Carmichael 1987) or directly uses the acoustic velocities of oxides (Schilling et al. 2001) to calculate elastic moduli of melts and glasses. We are not able to test the third method due to a lack of the data of sound speed coefficients and the acoustic velocities for all oxides we used, though Schilling et al. (2001) reported a nice ideal mixing behavior in their MgO–CaO–Al_2O_3–SiO_2 glasses at room temperature.

Originally, the partial molar volumes of oxides were almost all collected at high temperatures. Lange (1996) and Schilling et al. (2001) reported an ideal mixing behavior in density of the Na_2O–Al_2O_3–SiO_2 and MgO–CaO–Al_2O_3–SiO_2 glasses at room temperature using extrapolated V_i data. Our aluminosilicate glasses contain 9–11 oxides. The V_i value of all these oxides cannot

Table 4 Contribution of cations to the elastic moduli of rhyolitic glasses (relative to *G*0)

Difference *G*0–*Gx*	Percentage change of elastic modulus, (Δ*M*%)			Density change (%)	Δ*M*%/mol % of equivalent M^{+}		
	E	*K*	*G*		*E*	*K*	*G*
*G*0–*G*1	7.51	10.48	6.94	7.65	1.13	1.58	1.05
*G*0–*G*2	1.58	0.48	1.89	1.94	0.35	0.11	0.42
*G*0–*G*3	−7.51	−9.52	−6.94	5.50	−0.50	−0.64	−0.47

$\Delta M\% = ((M_{G0} - M_{Gx})/M_{G0}) \times 100$, where $x = 1, 2, 3$, and $M = E$ (Young's), K (bulk), G (shear) moduli. The data were based on the average moduli shown in Fig. 5. For the change of elastic moduli, the negative sign represents *G*0 is weakened by the presence of cations, and the others show strengthened

Table 5 The linear-extrapolated partial molar volume (V_i) of oxides at 25°C

Oxides	1	2	3	4	5	6	7	Ave.V_i
SiO_2	27.26	26.75	26.9	26.86	26.91	27.33	26.99	27.00
Al_2O_3	37.60	–	33.51	37.42	37.49	36.28	33.91	36.03
Fe_2O_3	–	43.96	29.63	–	–	31.2	–	34.93
FeO	–	13.46	9.64	–	–	7.95	–	10.35
MnO	–	13.92	–	–	–	–	–	13.92
MgO	10.26	12.15	7.85	7.2	–	8.89	–	9.27
CaO	12.58	16.36	12.56	11.39	–	11.43	–	12.86
Na_2O	21.58	28.67	−11.80[a]	18.31	18.27	18.84	18.19	20.64
K_2O	34.91	45.81	29.46	29.46	–	30.04	–	33.94
TiO_2	32.17	21.94	13.21[a]	–	–	10.34[a]	–	27.06
P_2O_5	69.15	–	–	–	–	–	–	69.15
Reference temperature for extrapolation, °C	750	1,400	1,400	750	1,100	1,600	1,400	

References: *1* Knoche et al. (1995), *2* Bottinga et al. (1982), *3* Lange and Carmichael (1987), *4* Lange (1997), *5* Lange (1996), *6* Stebbins et al. (1984), *7* Stein et al. (1986)
[a]Data were not adopted in averaging

be found in a single literature. Furthermore, the thermal expansion data for the same oxide are different in different literatures. In order to test the validity of the ideal molar mixing model for our samples at room temperature, we used the average of the extrapolated published data as listed in Table 5. Among the seven data sets, only the experiment in Knoche et al. (1995) was carried out over room temperature. Thus only the 25°C data extrapolated from those of Knoche et al. (1995) are the most reliable. Unfortunately, the data of iron oxides and MnO were not measured by Knoche et al. (1995). To calculate the density, we combined the data of Knoche et al. (1995) and that of the three oxides (FeO, Fe_2O_3, MnO) reported by Bottinga et al. (1982). The glass density was calculated from $\rho_g = \sum M_i x_i / \sum V_i x_i$, where M_i is the gram-formula weight of oxide i. A comparison between our measured sample densities and the calculated (modeled) data is shown in Fig. 8. Obviously, both sets of the calculated density do not display a good ideal

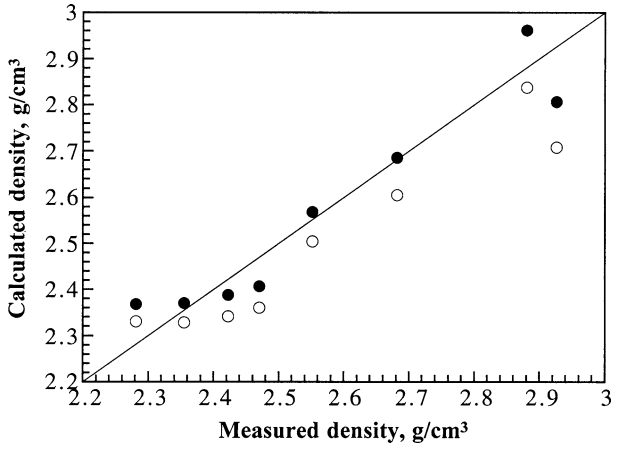

Fig. 8 Calculated versus measured densities for all aluminosilicate glasses used in this study. *Solid circles* denote the data calculated from the average extrapolated partial molar volumes listed in Table 5, and *open circles* denote the data calculated from Knoche et al. (1995) and Bottinga et al. (1982). The *diagonal* indicates ideal mixing behavior

mixing behavior, and the densities based on the average V_i show less deviation than that based on the data of Knoche et al. and Bottinga et al. A regular tendency between NBO/T and density deviation was also not found.

A direct calculation of Young's modulus of glass was first proposed by Makishima and Mackenzie (1973). The Young's modulus (E) is given as:

$$E(\text{GPa}) = \frac{2\rho_g[\sum(P_i x_i)\sum(G_i x_i)]}{M} \quad (8)$$

where P_i, G_i, and x_i are the packing factor, dissociation energy per unit volume and molar fraction of oxide i, respectively. M and ρ_g are the mean molar mass and density of the glass, respectively. By using Eq. 8, Makishima and Mackenzie (1973), Rocherulle et al. (1989), and Inaba et al. (1999) observed a good agreement between the modeled and measured Young moduli in their glasses. However, all P_i used in literature were based on Pauling's ionic radii in octahedral coordination, and the existing data of G_i are not enough for us to calculate Young's modulus of our samples. In addition, some authors have adopted the old thermodynamic data (Sun 1947; Sun and Huggins 1947) for their calculation of G_i. Therefore, we recalculated both P_i and G_i using Shannon's (1976) radii and the thermodynamic data listed in CRC Handbook of Chemistry and Physics (1992/1993), taking the appropriate coordination number of cations into consideration. The data of both P_i and G_i thus calculated are listed in Table 6. Two SiO_2 densities (quartz and amorphous silica) were considered in the calculation of G_i. Accordingly, the calculated (modeled) Youngs' moduli of our samples are compared with the measured moduli in Fig. 9a. Obviously, Youngs' moduli of our aluminosilicate glasses do not show an ideal mixing behavior. It is found that the deviation in the calculated Young's modulus is smaller at higher modulus region but larger in lower-modulus region when the density of quartz was used in the calculation. On the other hand, the opposite relationship was observed when the density of amorphous silica was

Table 6 Gram-formula weight (GFW), density, cationic radius, packing factor (P_i) and dissociation energy (G_i) of oxides used for calculation of the modeled Young's modulus of aluminosilicate glasses at ambient conditions

Oxides	GFW	Density[a] (g/cm^3)	Cationic radius[c] (Å)	Packing factor[d] (P_i cm^3/mol)	Dissociation energy[d] (G_i kJ/cm^3)
SiO_2 (low quartz)	60.085	2.647	0.26	13.89	81.57
SiO_2 (amorphous)	60.085	2.2[b]	0.26	13.89	67.80
Al_2O_3 (corundum)	101.962	3.987	0.39	21.07	119.57
Fe_2O_3 (hematite)	159.692	5.275	0.78	23.16	78.49
FeO (wüstite)	71.846	5.700	0.645	7.60	73.98
MnO (manganosite)	70.940	5.365	0.83	8.37	69.86
MgO (periclase)	40.304	3.576	0.72	7.86	91.16
CaO (lime)	56.077	3.343	1.00	9.45	60.51
α-Na_2O	61.979	2.394	1.02	12.28	31.90
α-K_2O	94.195	2.346	1.38	20.18	19.24
TiO_2 (rutile)	79.879	4.250	0.605	14.40	101.75
P_2O_5	141.945	2.463	0.17	34.64	56.69

[a]X-ray diffraction densities of crystals in JCPDS files were adopted
[b]The average density of amorphous silica is ca. 2.20 g/cm^3
[c]Data were from Shannon (1976). For calculation of P_i, tetrahedral coordination were adopted for Si^{4+}, Al^{3+}, and P^{5+} ions, while octahedral coordination for other cations and oxygen ion (1.40 Å). For Mn^{2+}, Fe^{2+}, and Fe^{3+}, the high-spin radii were adopted
[d]The P_i and G_i are defined as: $P_i(\mathrm{cm}^3/\mathrm{mol}) = 6.02 \times 10^{23} \times \frac{4}{3}\pi\left(Xr_M^3 + Yr_O^3\right)$ for oxide M_XO_Y and G_i (kJ/cm^3) = $\rho_i[X\ \Delta H_f(M, \text{gas}) + Y\Delta H_f(O, \text{gas}) - \Delta H_f(M_XO_Y, \text{crystal}) - (X+Y)RT]/M_i$, where x_i is the molar fraction of oxide i, R the gas constant, and T the temperature. M and M_i are the mean molar mass of the glass and the gram-formula weight of the oxide i, respectively. ρ_g and ρ_i are the densities of the glass and oxide i, respectively. r_M and r_O are the radii of M and O, respectively. ΔH_f(M, gas), ΔH_f(O, gas), and $\Delta H_f(M_XO_Y$, crystal) are the molar enthalpies of formation of gaseous M, O and crystalline oxide, respectively

used. The low-modulus region corresponds to the highly polymerized and silica-like rhyolitic glasses, while the higher-modulus corresponds to the less polymerized basaltic glasses. This suggests that density (or G_i) of SiO_2 is a crucial factor for obtaining a reasonable Young's modulus based on the ideal mixing model. From Fig. 9a, G_i of SiO_2 should not be a constant if the present aluminosilicate glasses follow an ideal mixing behavior. The differences between calculated and measured Young's modulus against NBO/T is displayed in Fig. 9b. Basically, the difference becomes more positive with decreasing NBO/T except for sample G3 (NBO/T = 0.111). This tendency is similar to that observed in the anorthite-diopside-forsterite glasses (Schilling et al. 2001), though negative deviation was displayed in that system. The abnormal behavior of G3 might be attributed to the dual role of Al^{3+} in the glasses. A part of Al^{3+} in G3 act as network former and a part of Al^{3+} are modifiers; the former is tetrahedrally coordinated and the latter is octahedrally coordinated. Different coordinations will result in different P_i and probably G_i.

From the above results and discussion, the ideal molar mixing model based on V_i, P_i, and G_i data cannot be applied to predict the elastic properties of the present glasses. The cause is complicated. For glass density, Schilling et al. (2001) attributed the small scatter of their modeled data to the uncertainty in density measurements. However, it is not the case of the present glasses because large deviation was observed. Several causes may interpret the large deviation in the calculated (modeled) density: (a) the thermal expansivities measured at high temperature cannot be linearly extrapolated to room temperature because the thermal expansivity of a glass is always far smaller than its corresponding melt, (b) V_i of an oxide is not a constant in all glass at a given temperature due to different interaction among oxides, and (c) the concentration and temperature dependences of melt's volume are not truly linear as that assumed in all measurements. All these factors will cause an incorrect estimation in V_i and thus glass density. Bottinga et al. (1982) pointed out that the V_i of Al_2O_3 depends on melt composition, while Lange (1996, 1997) reported that both SiO_2 and Al_2O_3 do not contribute to the thermal expansivity of the melts in the range of 701–1,896 K (note that all the V_i of Al_2O_3 in different melts studied by Lange are the same). The contradiction among these studies indicates that the effect of interaction between the constituent oxides should be case by case. Recently, a report based on 80 glasses has pointed out that the density of a Na_2O–Al_2O_3–SiO_2 glass is almost independent of the concentration of Al_2O_3 (Doweidar 1998). A recalculation on their data using the V_i data listed in Table 5 also shows a non-ideal mixing.

For Young's modulus of the glasses, the large deviation in calculated modulus has implied the following facts: (a) the dissociation energy of *crystalline* oxide cannot be used without a modification by considering the contribution of amorphization, (b) the coordination number of a cation in a glass and melt may not be identical to that in its crystalline phase because cations are apt to have lower coordination in glasses than in crystals (Calas et al. 2002), and (c) the interaction among oxides, the contribution from the field strength of cation, and effect of concentration cannot be neglected. These factors should significantly influence the G_i of an oxide in glass. The nonlinear composition dependences in elastic moduli of alkali silicate glasses (Lin et al. 2006) also indicates that (a) the G_i of an oxide should not be a constant and (b) an estimation of elastic moduli using

constant C_i as done by Rivers and Carmichael (1987) is not always valid. In brief, the present results indicate that an accurate estimation of density and elastic properties of a glass or melt based on the ideal mixing model and the known parameters (V_i, P_i, G_i, and C_i) is difficult, if it is not impossible.

Elastic modulus and viscosity of aluminosilicate melt at high temperature

According to Maxwell relationship, the shear viscosity of a viscoelastic substance is the product of its relaxation time and the shear modulus at infinite frequency (e.g. Askarpour and Manghnani 1993). Therefore, it is also of interest to understand qualitatively the possible correlation between shear modulus of a glass and the viscosity of its corresponding melt. The viscosity of many binary silicate glasses (e.g., M_2O–SiO_2 and $M'O$–SiO_2 systems, M = Li, Na, K, Rb, Cs, and M′ = Mg, Ca, Sr, Ba, Pb; Bansal and Doremus 1986) and diopside-albite aluminosilicate melts (in the range 1,350–1,550°C; Scarfe and Cronin 1986) has been found to decreases with increasing bulk NBO/T. Viscosity of a silicate melt also decreases with increasing the field strength of cations (Mysen 1988). Therefore, the melts (or glasses) containing more amounts of cations should show lower viscosity due to stronger effect of electric field in average.

From the DSC analysis, the peak temperatures for crystallization in the present basaltic glasses have the order: $B3$ (>950°C) > $B2$ (~930°C) > $B1$ (885°C) > $B0$ (840°C). Shimizu and Kushiro (1991) pointed out that the transport rates of all species in the diopside-jadeite aluminosilicate melts at 1,550°C and 10 kbar decrease with increasing in polymerization of the melt. If the crystalline phases formed in the present samples are the same, then the diffusion rates of cations and Q species at high temperature should have the order: $B3 < B2 < B1 < B0$. All these points have attained the conclusion that the viscosity of a basaltic melt would decrease with increasing NBO/T in the range 40–70 mol% SiO_2, and a glass with higher shear modulus will display a lower viscosity at high temperature if other major elements in a series of glasses are similar.

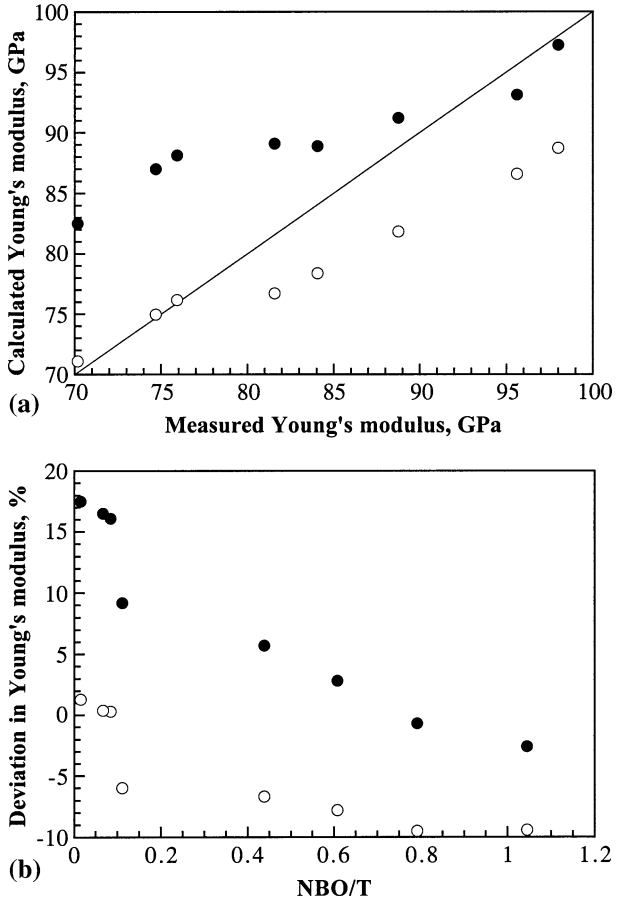

Fig. 9 **a** Young's modulus of aluminosilicate glasses measured in this study compared with that calculated from the model of Makishima and Mackenzie (1973) and **b** difference in the calculated Young's modulus and the measured values plotted as a function of NBO/T. *Open circles* denote the data calculated using the density of amorphous silica (2.2 g/cm^3) and *solid circles* using the density of quartz (2.647 g/cm^3). The deviation in Young's modulus is defined to be $100\times(E-E_m)/E_m$, where E and E_m are the calculated and measured moduli, respectively. The diagonal in (**a**) represents an ideal mixing behavior

Conclusions

Brillouin and Raman spectroscopy have been used to study the effects of composition and anionic structure on the elastic properties of both basaltic and rhyolitic glasses at ambient conditions. It has found that bulk, shear and Young's moduli of the basaltic glasses all decrease monotonically with increasing SiO_2 concentration when the relative amounts of other components remain the same. An analysis based on the relative abundance and geometry of Q species has revealed that bulk modulus of the basaltic glasses strongly depends on the sum of Q^3 and Q^4. In other words, the more the glass contains (Q^3 + Q^4), the more compressible it is. The significant difference in the change rates between shear and bulk moduli with SiO_2 content has been attributed to different mechanisms for compression and shear deformation in a glass.

For both types of glasses, the dependences of elastic moduli on bulk NBO/T indicates that the elastic modulus of a glass strongly depends on the effective concentration of modifying cations rather than the apparent concentration of all non-network-forming cations. For the rhyolitic glasses, it is found that iron oxides display the strongest effect on the elastic moduli. The major effect of alkaline earth cations is on shear modulus, and both iron and alkali cations have stronger effects on bulk modulus. Iron and alkali cations also show similarly relative contribution between both bulk and shear

moduli, indicating that the two types of cations may have similar local structure or prefer to associate with the same anionic units in the glass. For alkaline earth cations, the large difference in contribution between bulk and shear moduli implies that Mg^{2+} and Ca^{2+} prefer to associate with Q^2 and Q^1 rather than the more polymerized Q^3 and Q^4.

Furthermore, it is found that the ideal molar mixing model based on the partial molar volume, packing factor, and dissociation energy of oxides is failed in prediction of the elastic properties of our multicomponent aluminosilicate glasses. An accurate estimation of elastic properties using the ideal molar mixing model requires a consideration of other factors involving an improvement in the calculation of partial molar volume, packing factor, dissociation energy, and sound speed coefficients of oxides. Finally, a consideration of NBO/T, Z/r^2 field of cation, and crystallization temperature has led to the inference that the viscosity of the present basaltic glasses should have the order: $B3 > B2 > B1 > B0$ at elevated temperatures. In other words, the viscosity of a basaltic melt should increase with decreasing shear modulus of its corresponding glass in the range 40–70 mol% SiO_2.

Acknowledgments The authors thank the anonymous referee for helpful comments and Mr. T. S. Kao, Department of Chemistry of National Taiwan University, for the help with DSC experiments. This work was supported by National Science Council, Taiwan, R. O. C. under contacts NSC 90-2116-M-001-007 and NSC 91-2116-M-001-016.

References

Askarpour V, Manghnani MH (1993) Elastic properties of diopside, anorthite, and grossular glasses and liquids: a Brillouin scattering study up to 1400 K. J Geophys Res 98B:17683–17689

Bansal NP, Doremus RH (1986) Handbook of glass properties. Academic, San Diego, 680 p

Bottinga Y, Weill D, Richet P (1982) Density calculations for silicate liquids. I. Revised method for aluminosilicate compositions. Geochim Cosmochim Acta 46:909–919

Burkhard DJM (1997) Elastic properties of alkali silicate glasses with iron oxide: relation to glass structure. Solid State Commun 101:903–907

Calas G, Cormier L, Galoisy L, Jollivet P (2002) Structure-property relationships in multicomponent oxide glasses. C R Chim 5:831–843

Domine F, Piriou B (1986) Raman spectroscopic study of the SiO_2–Al_2O_3–K_2O vitreous system: distribution of silica and second neighbors. Amer Mineral 71:38–50

Doweidar H (1998) Density-structure correlations in Na_2O–Al_2O_3–SiO_2 glasses. J Non-Cryst Solids 240:55–65

Furukawa T, White WB (1979) Structure and crystallization of glasses in the $Li_2Si_2O_5$–TiO_2 system determined by Raman spectroscopy. Phys Chem Glasses 20:69–80

Galeener FL (1979) Band limits and the vibrational spectra of tetrahedral glasses. Phys Rev B19:4292–4297

Gavriliu G (2001) Effects of added oxide and thermal history on Young's modulus of added oxide(s)–Na_2O–SiO_2 glass. Mater Lett 48:199–204

Inaba S, Fujino S, Morinaga K (1999) Young's modulus and compositional parameters of oxide glasses. J Amer Ceram Soc 82:3501–3507

Iwamoto N, Tsunawaki Y, Fuji M, Hatfori T (1975) Raman spectra of K_2O–SiO_2 and K_2O–SiO_2–TiO_2 glasses. J Non-Cryst Solids 18:303–306

Karlsson KH, Fröberg K (1987) Structural units in silicate glasses. Chem Geol 62:1–5

Knoche R, Dingwell DB, Webb SL (1995) Melt densities for leucogranites and granitic pegmatites: partial molar volumes for SiO_2, Al_2O_3, Na_2O, K_2O, Li_2O, Rb_2O, Cs_2O, MgO, CaO, SrO, BaO, B_2O_3, P_2O_5, F_2O_{-1}, TiO_2, Nb_2O_5, Ta_2O_5, and WO_3. Geochim Cosmochim Acta 59:4645–4652

Konijnendijk WL, Stevelts JM (1976) Raman scattering measurements of silicate glasses and compounds. J Non-Cryst Solids 21:447–453

Kushiro I (1975) On the nature of silicate melt and its significance in magma genesis: regularities in the shift of liquidus boundaries involving olivine, pyroxene, and silica materials. Amer J Sci 275:411–431

Lange RA (1996) Temperature independent thermal expansivities of sodium aluminosilicate melts between 713 and 1835 K. Geochim Cosmochim Acta 60:4989–4996

Lange RA (1997) A revised model for the density and thermal expansivity of K_2O–Na_2O–CaO–MgO–Al_2O_3– SiO_2 liquids from 700 to 1900 K: extension to crustal magmatic temperatures. Contrib Mineral Petrol 130:1–11

Lange RA, Carmichael ISE (1987) Densities of Na_2O–K_2O–CaO–MgO–FeO– Fe_2O_3–Al_2O_3 –TiO_2–SiO_2 liquids: new measurements and derived partial molar properties. Geochim Cosmochim Acta 51:2931–2946

Le Saoût G, Vaills Y, Luspin Y (2002) Effects of thermal history on mechanical properties of $(PbO)_x(ZnO)_{0.6-x}(P_2O_5)_{0.4}$ glasses using Brillouin scattering. Solid State Commun 123:49–54

Li CC (2004) Effects of cation size and anionic structure on the elasticity of alkali and alkaline earth silicate glasses. MS Thesis, Institute of Materials and Mineral Resource Engineering, National Taipei University of Technology

Lin CC, Shen P, Chang HM, Yang YJ (2006) Composition dependent structure and elasticity of lithium silicate glasses: Effect of ZrO_2 additive and the combination of alkali silicate glasses. J Eur Ceram Soc (in press)

Makishima A, Mackenzie JD (1973) Direct calculation of Young's modulus of glass. J Non-Cryst Solids 12:35–45

McMillan P (1984) A Raman spectroscopic study of glasses in the system CaO–MgO–SiO_2. Amer Mineral 69:645–659

McMillan PF, Wolf GM (1995) Vibrational spectroscopy of silicate liquids. In: Stebbins JF, MaMillan PF, Dingwell DB (eds) Structure, dynamics and properties of silicate melts. Mineralogical Society of America, Washington DC, pp 247–315

McMillan P, Piriou B, Navrotsky A (1982) A Raman spectroscopic study of glasses along the joins silica-calcium aluminate, silica-sodium aluminate, and silica-potassium aluminate. Geochim Cosmochim Acta 46:2021–2037

Mysen BO (1987) Magmatic silicate melts: Relations between bulk composition, structure and properties. In: Mysen BO (ed) Magmatic processes: physicochemical principles. The Geochemical Society, Penn, pp 375–399

Mysen BO (1988) Structure and properties of silicate melts. Elsevier, Amsterdam, 354 p

Mysen BO (2003) Physics and chemistry of silicate glasses and melts. Eur J Mineral 15:781–802

Mysen BO, Virgo D, Scarfe CM (1980a) Relations between the anionic structure and viscosity of silicate melts—a Raman spectroscopic study. Amer Mineral 65:690–710

Mysen BO, Ryerson FJ, Virgo D (1980b) The influence of TiO_2 on the structure and derivative properties of silicate melts. Amer Mineral 65:1150–1165

Mysen BO, Ryerson FJ, Virgo D (1981a) The structural role of phosphorus in silicate melts. Amer Mineral 66:106–117

Mysen BO, Virgo D, Kushiro I (1981b) The structural role of aluminum in silicate melts—a Raman spectroscopic study at 1 atmosphere. Amer Mineral 66:678–701

Mysen BO, Finger L, Virgo D, Seifert FA (1982) Curve-fitting of Raman spectra of silicate glasses. Amer Mineral 67:686–695

Navrotsky A, Peraudeau P, McMillan P, Coutoures JP (1982) A thermochemical study of glasses and crystals along the joins silica–calcium aluminate and silica–sodium aluminate. Geochim Cosmochim Acta 46:2039–2049

Poe BT, McMillan PF, Angell CA, Sato RK (1992) Al and Si coordination in SiO_2–Al_2O_3 glasses and liquids: a study by NMR and IR spectroscopy and MD simulations. Chem Geol 96:333–349

Rivers ML, Carmichael ISE (1987) Ultrasonic studies of silicate melts. J Geophys Res 92B:9247–9270

Rocherulle J, Ecolivet C, Poulain M, Verdier P, Laurent Y (1989) Elastic moduli of oxynitride glasses: extension of Makishima and Mackenzie's theory. J Non-Cryst Solids 108:187–193

Rouse GB, Kamitsos EI, Risen WM Jr (1981) Brillouin spectra of mixed alkali glasses: $x Cs_2O(1–x)Na_2O5SiO_2$. J Non-Cryst Solids 45:257–269

Ryerson FJ (1985) Oxide solution mechanisms in silicate melts: systematic variations in the activity coefficient of SiO_2. Geochim Cosmochim Acta 49:637–651

Ryerson FJ, Hess PC (1980) The role of P_2O_5 in silicate melts. Geochim Cosmochim Acta 44:611–624

Scarfe CM, Cronin DJ (1986) Viscosity-temperature relationships of melts at 1 atm in the system diopside-albite. Amer Mineral 71:767–771

Schilling FR, Hauser M, Sinogeikin SV, Bass JD (2001) Compositional dependence of elastic properties and density of glasses in the system anorthite-diopside-forsterite. Contrib Mineral Petrol 141:297–306

Schilling FR, Sinogeikin SV, Hauser M, Bass JD (2003) Elastic properties of model basaltic melt compositions at high temperatures. J Geophys Res 108(B6):ECV 9 1–13

Schreiber HD, Kochanowski BK, Schreiber CW, Morgan AB, Coolbaugh MT, Dunlap TG (1994) Compositional dependence of redox equilibria in sodium silicate glasses. J Non-Cryst Solids 177:340–346

Schroeder J, Mohr R, Macedo PB, Montrose CJ (1973) Rayleigh and Brillouin scattering in K_2O–SiO_2 glasses. J Amer Ceram Soc 56:510–514

Shannon RD (1976) revised effective ionic radii and systematic studies of interatomic distances in halides and chalcogenides. Acta Cryst A32:751–767

Shimizu N, Kushiro I (1991) The mobility of Mg, Ca, and Si in diopside-jadeite liquids at high pressures. In: Perchuk LL, Kushiro I (eds) Physical chemistry of magma. Springer, Berlin Heidelberg New York, pp 192–212

Stebbins JF, Carmichael ISE, Moret LK (1984) Heat capacities and entropies of silicate liquids and glasses. Contrib Mineral Petrol 86:131–148

Stebbins JF, Murdoch JB, Schneider E, Carmichael ISE, Pines A (1985) A high-temperature high-resolution NMR study of ^{23}Na, ^{27}Al and ^{29}Si in molten silicates. Nature 314:250–252

Stein DJ, Stebbins JF, Carmichael ISE (1986) Density of molten sodium aluminosilicates. J Amer Ceram Soc 69:396–399

Sun K-H (1947) Fundamental condition of glass formation. J Amer Ceram Soc 30:277–281

Sun K-H, Huggins ML (1947) Energy additivity in oxygen-containing crystals and glasses. II. J Phys Colloid Chem 5:438–443

Taylor M, Brown GE (1979) Structure of mineral glasses. I. The feldspar glasses $NaAlSi_3O_8$, $KAlSi_3O_8$, $CaAl_2Si_2O_8$. Geochim Cosmochim Acta 43:61–77

Vaills Y, Luspin Y, Hauret G, Coté B (1996) Two opposite effects of sodium on elastic constants of silicate binary glasses. Mater Sci Eng B40:199–202

Vaills Y, Luspin Y, Hauret G (2001) Annealing effects in SiO_2–Na_2O glasses: investigation by Brillouin scattering. J Non-Cryst Solids 86:224–234

Vo-Thanh D, Polian A, Richet P (1996) Elastic properties of silicate melt up to 2350 K from Brillouin scattering. Geophys Res Lett 23:423–426

Whitfield CH, Brody EM, Bassett WA (1976) Elastic moduli of NaCl by Brillouin scattering at high pressure in a diamond anvil cell. Rev Sci Instrum 47:942–947

Yamane M, Okuyama M (1982) Coordination number of aluminum ions in alkali-free alumino-silicate glasses. J Non-Cryst Solids 52:217–226